Materials Science & Engineering C 113 (2020) 110998

Contents lists available at ScienceDirect

Materials Science & Engineering C

journal homepage: www.elsevier.com/locate/msec

Nanodecoration of electrospun polymeric fibers with nanostructured silver coatings by ionized jet deposition for antibacterial tissues

Giorgia Pagnotta[a], Gabriela Graziani[b], Nicola Baldini[b,c], Alessandra Maso[d], Maria Letizia Focarete[a,e], Matteo Berni[b,1], Fabio Biscarini[f,g], Michele Bianchi[f,*], Chiara Gualandi[a,h,**]

[a] Department of Chemistry "Giacomo Ciamician" and INSTM UdR of Bologna, University of Bologna, Via Selmi, 2, 40126 Bologna, Italy
[b] IRCSS Istituto Ortopedico Rizzoli, Laboratorio NanoBiotecnologie (NaBi), Via di Barbiano 1/10, 40136 Bologna, Italy
[c] Department of Biomedical and Neuromotor Sciences, University of Bologna, Via Foscolo 7, 40123 Bologna, Italy
[d] IRCSS Istituto Ortopedico Rizzoli, Quality Control in GMP, Via di Barbiano 1/10, 40136 Bologna, Italy
[e] Health Sciences & Technologies (HST) CIRI, University of Bologna, Via Tolara di Sopra 41/E, 40064 Ozzano Emilia, Bologna, Italy
[f] Center for Translational Neurophysiology of Speech and Communication, Istituto Italiano di Tecnologia, Via Fossato di Mortara, 17-19, 44121 Ferrara, Italy
[g] Life Science Department, University of Modena and Reggio Emilia, Via Giuseppe Campi 287, 41125 Modena, Italy
[h] Interdepartmental Center for Industrial Research on Advanced Applications in Mechanical Engineering and Materials Technology, CIRI-MAM, University of Bologna, Viale Risorgimento, 2, 40136 Bologna, Italy

ARTICLE INFO

Keywords:
Electrospinning
Ionized jet deposition
Silver coating
Nanostructured coating
Wound dressing

ABSTRACT

Silver-based nanomaterials are used as antibacterial agents in a number of applications, including wound dressing, where electrospun materials can effectively promote wound healing and tissue regeneration thanks to their biomimicry, flexibility and breathability. Incorporation of such nanomaterials in electrospun nonwovens is highly challenging if aiming at maximizing stability and antibacterial efficacy and minimizing silver detachment, without neglecting process straightforwardness and scalability. In this work nanostructured silver coatings were deposited by Ionized Jet Deposition (IJD) on Polylactic acid, a medical grade polyester-urethane and Polyamide 6,6 nanofibers. The resulting materials were thoroughly characterized to gain an in-depth view of coating morphology and substrate resistance to the low-temperature deposition process used. Morphology of silver coatings with well-cohesive grains having dimensions from a few tens to a few hundreds of nanometers was analyzed by SEM, TEM and AFM. TGA, DSC, FTIR and GPC showed that the polymers well withstand the deposition process with negligible effects on their properties, the only exception being the polylactic acid that resulted more susceptible to degradation. Finally, the efficacy against *S. aureus* and *E. coli* bacterial strains was demonstrated, indicating that electrospun fibers decorated with nanostructured silver by IJD represent a breakthrough solution in the field of antibacterial devices.

1. Introduction

Silver (Ag) is the most common inorganic antibacterial agent employed in wound care and in prevention of infection. Its wide use is due to its efficacy against several strains of bacteria, including drug-resistant ones, and its capability of preventing biofilm formation of biofilms that are responsible for impaired wound healing [1]. In particular, either Ag coatings and silver nanoparticles (AgNPs) are extensively used, due to Ag capability of directly damaging bacteria membranes and subcellular structures, preventing cell adhesion and/or biofilm formation at the wound surface [2]. Moreover, effective wound dressing materials should also be able to i) preserve the volume and shape of the native tissue, ii) maintain a suitable environment at the wound/dressing interface by absorbing the excess exudate and preventing leakage towards the dressing surface and iii) allow gaseous and fluid exchange. Finally, wound dressing materials should promote the biological cascades of events eventually leading to a complete tissue regeneration without causing adverse reactions, such as inflammation [3,4].

* Corresponding author.
** Correspondence to: C. Gualandi, Department of Chemistry "Giacomo Ciamician" and INSTM UdR of Bologna, University of Bologna, Via Selmi, 2, 40126 Bologna, Italy.
E-mail addresses: michele.bianchi@iit.it (M. Bianchi), gualandi@unibo.it (C. Gualandi).
[1] Present Address: IRCCS Istituto Ortopedico Rizzoli, Laboratorio di Tecnologia Medica, Bologna, Italy.

https://doi.org/10.1016/j.msec.2020.110998
Received 17 February 2020; Received in revised form 27 March 2020; Accepted 20 April 2020
Available online 23 April 2020

In this framework, great attention has been paid to electrospun polymeric nanofibers [5–7], as they can mimic the skin native structure, which is characterized by an extracellular matrix composed of continuous fibers with diameters at the nanoscale. The great potentialities of electrospun mats as wound dressings have been largely demonstrated and are specifically linked to their ability to respond to the above mentioned requirements, by draining wound exudates, allowing oxygen exchange, adapting to complex wound contours and preventing scar tissue formation by promoting the regeneration of normal skin [8–10].

Among the different approaches adopted to confer antimicrobial properties to the electrospun mats, the development of hybrid AgNPs/polymer nanofibers composites has been heavily investigated [5,11]. The incorporation of nanoparticles (NPs) into fibers is commonly achieved either by direct dispersion or by in situ generation of NPs in solution [12–17]. Nevertheless, the simplicity of these approaches is accompanied by some drawbacks, such as possible aggregation of particles and the incorporation of the majority of NPs in the bulk of the electrospun fibers, with only few available on the surface, prone to interact with bacteria [11]. With the specific aim of enhancing antibacterial efficiency, other methods have been therefore applied to develop hybrid nanoparticle-enriched fibers, including co-axial electrospinning [18–20], in situ formation of AgNPs through either chemical [21,22] or physical treatments [23,24], and immersion of pre-fabricated non-wovens into AgNPs solution [25–27], sometimes previously treated with plasma to favor particle attachment [28]. In other examples, different chemical treatments have been applied to produce silver-based surface nanostructures [29,30]. Although these approaches can successfully produce materials with effective antimicrobial properties, they suffer from limited reproducibility, low control over film thickness and from NPs detachment, possibly leading to cytoxocity and/or inflammation. Indeed, coating of electrospun fibers with silver can be challenging. First, if carried out in water solution, electrospun mats frequently need previous treatments to be wetted [25,31,32]. Other organic solvents can be used, provided that they do not remain trapped inside the fiber, causing cytotoxicity. Then, the deposition must occur at low temperature, to minimize polymer degradation and damage of the fibers. In addition, the coating must have reproducible characteristics in terms of thickness, surface morphology and composition. Thickness of the silver coating must be at the sub-micrometric scale, to avoid detachment from the fibers. Finally, the coating must grow around the fiber, without occluding fabric porosity or significantly altering the fibrous shape. At present, no satisfactory options are available to address all these aims simultaneously.

In this work we propose a new straightforward strategy for the production of nanostructured antibacterial silver coatings on polymeric nanofibers obtained by combining the well-established electrospinning process with the novel Ionized Jet Deposition (IJD) technique. IJD is a Physical Vapour Deposition (PVD) technique in which ablation and subsequent deposition of thin films of a target material is achieved by an ultra-fast (100 ns), highly energy (10 J) and high density (10^9 W cm^{-2}) pulsed electron beam [33,34]. IJD has been emerging as an industrially feasible an effective approach able to produce highly adherent, homogeneous and nanostructured thin films of different classes of materials (metallic and ceramic targets, including complex ion-doped ceramics), with a high adhesion to the substrate and a fine control over film thickness and surface morphology [35–40]. IJD is normally used to coat metallic and ceramic substrates, while few studies are reported on more chemically and thermally sensitive materials, like polymers [41]. Deposition of nanostructured Ag thin coatings by IJD has been very recently reported, with promising results [42], but deposition on heat-sensitive and/or porous/fibrous substrates has not yet been investigated.

In this work, Ag coatings have been deposited by IJD onto three classes of biocompatible polymers commonly used as wound dressing materials and exhibiting different chemical and mechanical properties, namely a medical-grade polyester-urethane (PU), an aliphatic polyamide (PA 6,6) and a polyester, i.e. polylactic acid (PLLA). The effect of coating deposition process on fiber morphology, composition and thermal properties have been thoroughly investigated to assess the feasibility of the technique in nanodecorating polymeric nanofiber surface. Finally, agar diffusion antibacterial tests with *S. aureus* and *E. coli* strains have been carried out to preliminary assess the antibacterial efficacy of the proposed approach.

2. Experimental details

2.1. Materials

Poly(L-lactic acid) (PLLA) (Lacea H.100-E) was purchased from Mitsui Fine Chemicals. Nylon 6,6 Zytel® E53 (PA 6,6) was kindly provided by DuPont. Desmopan® 2590A medical grade polyester polyurethane (PU) was kindly provided by Bayer. Dichloromethane (DCM, Sigma Aldrich, ≥99.8%), *N*,*N*-dimethylformamide (DMF, Sigma Aldrich, ≥99.8%), 1,1,1,3,3,3-Hexafluoro-2-propanol (HFP, Sigma Aldrich, ≥99%) and ethanol (96%, Carlo Erba) were used without further purification. Pure metallic silver disks (2.00″ Diameter × 0.250″ Thickness, 99.99% purity, Kurt J Lesker, USA) were used as deposition targets, to manufacture the Ag coatings.

2.2. Electrospinning

The home-made electrospinning apparatus is composed of a SL 50 P 10/CE/230 high voltage power supplier (Spellman, New York, USA), a KDS-200 syringe pump (KDScientific Inc., Massachusetts, USA), a glass syringe containing the polymer solution, a stainless-steel blunt-ended needle (Hamilton, Bonaduz, Switzerland) connected with the power supply electrode and a grounded cylindrical aluminum collector (length = 10 cm, diameter = 5 cm, rotating at 50 rpm). The polymer solution was dispensed through a Teflon tube to the needle that was orthogonally placed on the rotating cylindrical collector. To fabricate PU mats the starting polymeric solution was prepared by dissolving 7% *w/v* of Desmopan 2590A in HFP, by using a G24 needle and by applying a voltage of 13 kV, a needle-to-collector distance of 20 cm and a flow rate of 1.2 mL/h. PLLA was electrospun starting from a polymer solution at 13% *w/v* in a mixture of DCM:DMF = 65:35 *v*/v, by using a G21 needle and by applying a voltage of 17 kV, a needle-to-collector distance of 20 cm and a flow rate of 1.4 mL/h. PA 6,6 nanofibers were obtained starting from a polymer solution at 20% w/v in HFP by using a G24 needle and by applying a voltage of 20 kV, a needle-to-collector distance of 15 cm and a flow rate of 0.5 mL/h. The obtained electrospun mats had a final dimension of about 15 × 8 cm^2 and a thickness in the range 70–100 μm.

2.3. Deposition of silver nanostructured coatings by ionized jet deposition

Ag thin films were deposited on the surface of the polymer patches by an Ionized Jet Deposition system (Noivion Srl, Rovereto (TN), Italy) [43], using metallic silver as target. Before deposition, the vacuum chamber was evacuated down to a base pressure of 1.0×10^{-7} mbar by a turbo-molecular pump (EXT255H, Edwards, Crawley, England) and then raised by controlled flow of oxygen (purity level = 99.999%) to 1.2×10^{-4} mbar. The electron beam working voltage and frequency were set at 22 kV and 7 Hz, respectively. To ensure a uniform and homogeneous deposition on multiple samples, both the target and the substrates were mounted on a rotating holder set 8 cm apart one from each other and a low deposition rate (≈2–3 nm/min) was maintained to avoid over heating of the polymeric patches. Ag-coated fibers were labelled according to the substrate material as Ag-PLLA, Ag-PA 6,6 and Ag-PU. Deposition time is an essential parameter in IJD deposition, as it determines film thickness and surface nanostructuration and, in turn, silver release, efficacy and cytotoxicity. Here, deposition time was selected based on preliminary unpublished results obtained for flat glass

substrates, aimed at determining a range of thickness/deposition times allowing good antibacterial efficacy while avoiding cytotoxicity. Deposition times below 20 min did not show antibacterial efficacy, while some cytotoxicity was evidenced above 60 min. Accordingly, optimal deposition time was selected in the range of 20 min and 60 min. An intermediate value of 40 min was thus selected in this work. For Ag-PLLA that exhibited significant damage as a result of deposition, a shorter deposition time (20 min) was also examined.

2.4. Characterization techniques

Scanning electron microscopy (SEM) coupled with Energy Dispersion X-ray Spectroscopy (EDS) was carried out by using a Leica Cambridge Stereoscan 360 scanning electron microscope at an accelerating voltage of 20 kV, before and after silver deposition. Samples were sputter-coated with gold prior to SEM observations. EDS was performed on unsputtered samples to determine sample composition through the acquisition of three spectra for each sample. The distribution of fiber diameters was determined through the measurement of about 300 fibers and the results were given as the average diameter ± standard deviation (SD). The one-way ANOVA was used to test the statistical significance of the difference between the mean values ($p < 0.001$).

Atomic Force Microscopy (AFM) was performed to gain more insights about the micro- and nanostructured surface of the coating on top of the fibers. AFM images were captured in air, at room temperature and in tapping mode using a Park XE7 AFM System (Park Systems, Suwon, Korea), equipped with non-contact Al-coated silicon cantilevers (tip radius < 10 nm, force constant ~42 N/m, resonant frequency ~330 kHz). Images were acquired at different scanning size, from 10 × 10 μm^2 to 0.8 × 0.8 μm^2 and elaborated with XEI software (Park Systems, Suwon, Korea).

Transmission Electron Microscopy (TEM) observations were carried out both on coated and uncoated samples by using a Philips microscope with an acceleration voltage of 80 kV. The fibers were electrospun directly on a TEM copper grid (100 mesh) and subsequently coated with silver through IJD. To verify the cohesion of silver coating to the fibers, the grids were immersed overnight in organic solvent prior to observations with the aim to dissolve only the polymeric component. In particular, Ag-PU and Ag-PA 6,6 were immersed in HFP while Ag-PLLA was kept in DCM.

Thermogravimetric analyses (TGA) were carried out using a TGA Q500 thermogravimetric analyzer (TA Instruments). Analyses were performed from RT to 800 °C, at a heating rate of 10 °C/min, under air flow.

Thermal transitions were measured by means of a differential scanning calorimeter (DSC Q100; TA Instruments), equipped with a refrigerated cooling system (RCS). Samples were subjected to two heating scans at 20 °C/min and one controlled cooling at 10 °C/min, applied between the heating scans. In particular, the following procedures have been used: for PLLA heating ramps from −40 °C to 210 °C and cooling ramp from 210 °C to −40 °C; for PU heating ramps from −90 °C to 210 °C and cooling ramp from 210 °C to −90 °C; for PA 6,6 heating ramps from −30 °C to 290 °C and cooling ramp from 290 °C to −30 °C.

FT-IR was carried out through Spectrum Two instrument equipped with ATR accessory (Perkin-Elmer, diamond crystal) on both silver coated and uncoated electrospun polymeric materials. All spectra have been registered between 400 cm^{-1} and 4000 cm^{-1} with a resolution of 4 cm^{-1}, accumulation 16 scans and step size 1 cm^{-1}.

Stress-strain measurements were performed with an Instron 4465 tensile testing machine on rectangular sheets cut from electrospun mats. Sample were 5 mm wide, the gauge length was 20 mm and the cross-head speed was 10 mm/min. Thickness was measured for each specimen by using a microcaliper. Load-displacement curves were obtained and converted to stress strain curves. At least ten replicate specimens were run for each sample and results were provided as the average value ± standard deviation.

Gel permeation chromatography (GPC) was carried out by using a KNAUER system equipped with a refractive index detector and two PL gel MiniMix C + a PL gel MiniMix E columns (250 mm/4.6 mm length/i.d.). Tetrahydrofuran was used as eluent with a 0.3 mL/min flow and sample concentrations of about 1 mg/mL. The analyzed samples were solubilized in tetrahydrofuran, stirred overnight and filtered on 0.20 μm PTFE filter. A molecular weight calibration curve was obtained with polystyrene standards in the range of molecular weight 2000–1,000,000 g/mol.

2.5. Antibacterial tests

Antibacterial tests were performed to evaluate the antibacterial efficacy of Ag-coated and uncoated electrospun mats. Before testing, square patches (1 × 1 cm^2) for each electrospun mat ($N = 3$) were sterilized by rinsing in ethanol (5 min), and dried at room temperature overnight. Gram-negative (*E. coli* ATCC 25922) and Gram-positive (*S. aureus* ATCC 25923) bacterial strains were used. Tests were performed in triplicate. The agar disk diffusion test according to Kirby-Bauer method was used. Briefly, the inoculum suspension was prepared selecting several colonies from over-night growth, suspending the colonies in sterile saline (0.85% NaCl *w/v* in water) to the density of a McFarland 0.5 standard turbidity (Densimat, Biomerieux), approximately corresponding to 1–2 × 10^7 CFU/mL. The inoculum was spread evenly over the entire surface of the un-supplemented Mueller Hinton (MH) agar plates (Vacutest Kima, Padua, IT, 90 mm) by swabbing in three directions. The coated and uncoated patches were deposited on the bacterial cultures, placing the coated side in direct contact with the bacterial suspension, and incubated in aerobiosis for 24 h at 35 ± 2 °C. At the end of the test, the diameters of the inhibition zone diameter (IZD) was evaluated in order to assess the antimicrobial efficacy of the silver coated fibers. Data were presented as mean ± standard deviation. Differences between groups were analyzed by a two-sample Student's *t*-test. Significance was set at $p < 0.05$.

3. Results and discussion

Non-wovens of randomly oriented nanofibers of PU, PA 6,6 and PLLA were fabricated by applying optimized electrospinning conditions to gain continuous, smooth and bead-free fibers (Fig. 1) with comparable sub-micrometric diameters (0.7 ± 0.2 μm for PU, 0.77 ± 0.09 μm for PA 6,6 and 0.7 ± 0.2 μm for PLLA, histograms in Fig. S1) that were used to investigate the effect of IJD silver deposition on materials that differ in the chemical structure while possessing the same microstructure and morphology. All non-wovens were highly flexible and resist to handling and folding. Their mechanical properties were determined by stress-strain measurements (Fig. S2 and Table S1) and results highlighted that PLLA is the strongest material with the higher elastic modulus (E = 102 MPa) and the lowest elongation at break (ε_b = 57%), PU is the more flexible one (E = 5 MPa) and can withstand higher deformations before rapture (ε_b = 260%), while PA 6,6 has intermediate value of elastic modulus (E = 31 MPa) and good deformation at break (ε_b = 115%).

To confer antibacterial properties to the polymeric mats, nanosilver coatings were deposited on the surface of the fibers by ablating a pure metallic silver target with a highly energetic pulsed electron beam. Inside the generated plasma plume, the ablated material is composed by silver ions, atoms, and larger clusters which start to coalesce within the plasma, and then adhere to the surface of the substrate, increase their size by apposition of other incoming material, giving rise to a continuous nanostructured film coating, mainly composed by metallic Ag [42]. Such a kind of coatings are similar to traditional coatings largely applied in the clinical practice, but with a sub-micrometric thickness and a highly rough surface morphology.

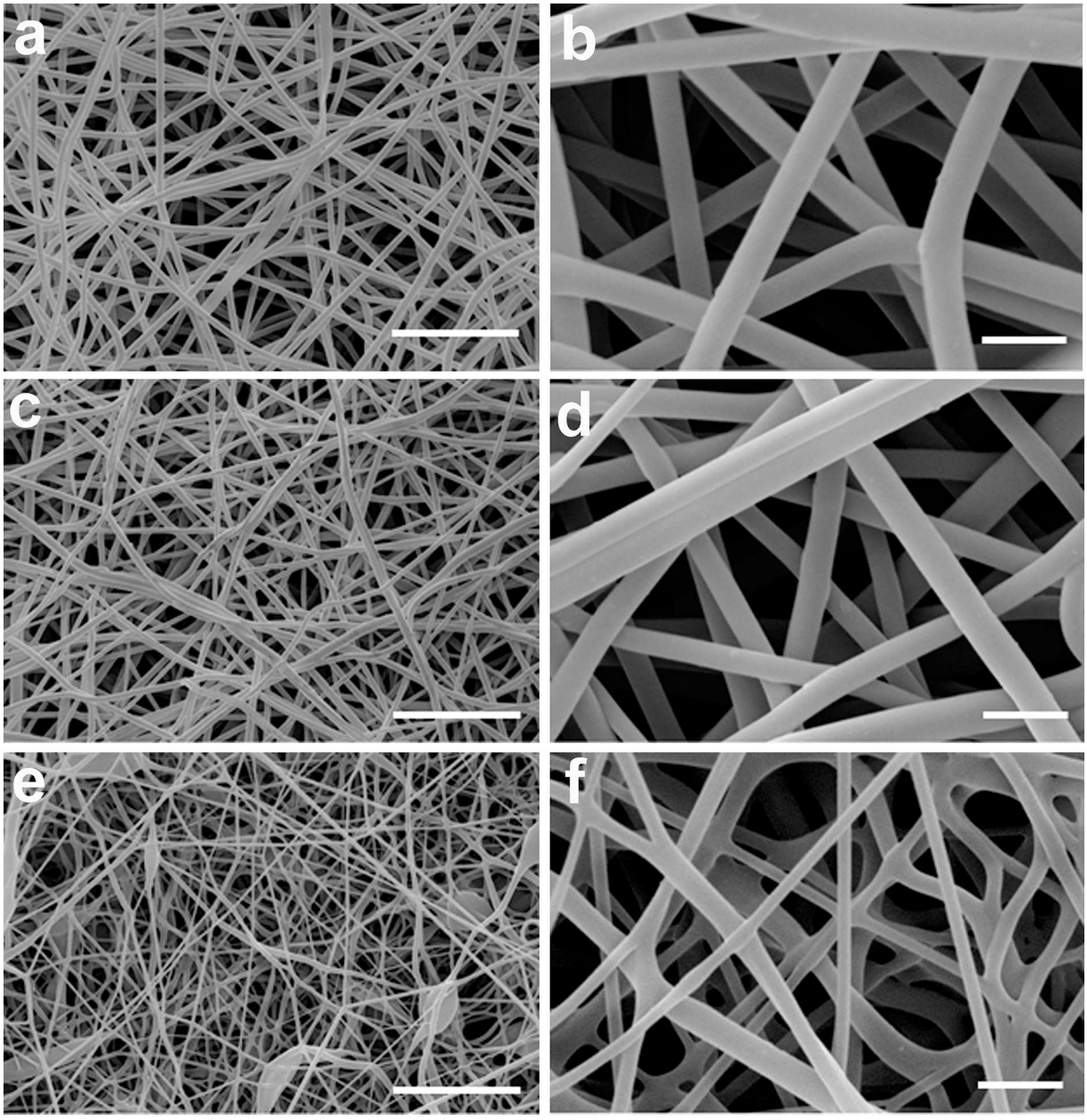

Fig. 1. SEM micrographs of electrospun nanofibers: (a, b) PU, (c, d) PA 6,6 and (d, e) PLLA. Scale bars: a, c, e = 10 μm; b, d, f = 3 μm.

After deposition, all samples acquired a homogeneous and intense silver coloring (Fig. S3). From a gross evaluation of the coating and of the mat mechanical stability, Ag-PU and Ag-PA 6,6 maintained their good handling and flexibility, without showing neither silver detachment when bended nor other relevant macroscopic modifications. Differently, Ag-PLLA clearly became more fragile, and easily fractured when bended, thus appearing to be damaged by the IJD treatment. In addition, the silver coating easily detached from the mat surface when the latter was bended. Consistently with the gross evaluations, SEM micrographs of coated mats (Fig. 2) showed that the deposition process did not affect the microscopic 3D morphology (porosity, fiber size) of the PU and PA 6,6 mats (Fig. 2a and c), but the presence of granular deposits could be detected on the surface of the fibers (Fig. 2b and d). Conversely, the 3D morphology of the coated PLLA mat was visibly modified (Fig. 2e and f); here, fibers appeared fused together in many points and the vast majority of the pores were occluded. A lower magnification image of Ag-PLLA sample reported in Fig. S4 clearly shows that in this mat Ag has well penetrated in the mat, generating a thick layer of fibers embedded in a continuous matrix of Ag. These qualitative observations were confirmed by both EDS analysis and by TGA analysis: EDS analysis (Fig. 2g, h, i, Table S2) indicated a higher amount of silver on the surface of PLLA fibers compared to PU and PA6, 6 (Ag content was 63, 21 and 23 wt%, respectively); the residual weight at high T in TGA (Fig. S5, Table S3) that provided an estimation of the silver amount in the whole sample, was 10, 4 and 6 wt% for PLLA, PU and PA 6,6, respectively. The higher amount of silver on PLLA mats may be related to the highly negative surface charge displayed by electrospun PLLA compared to the other two polymers [44–46], promoting attraction of positive ions generated in the plasma plume onto the fiber surface during the plasma deposition process. The formation of such a thick layer of silver may be advantageous in terms of bactericide effect but it is highly detrimental for coating stability that turned out to be very low in the case of PLLA, as previously described. Microscopic inspection of the fracture (Fig. S4) highlights that the detachment of Ag coating from PLLA mat surface is probably the consequence of cohesive failure. Indeed, it can be speculated that the coating rapture occurs

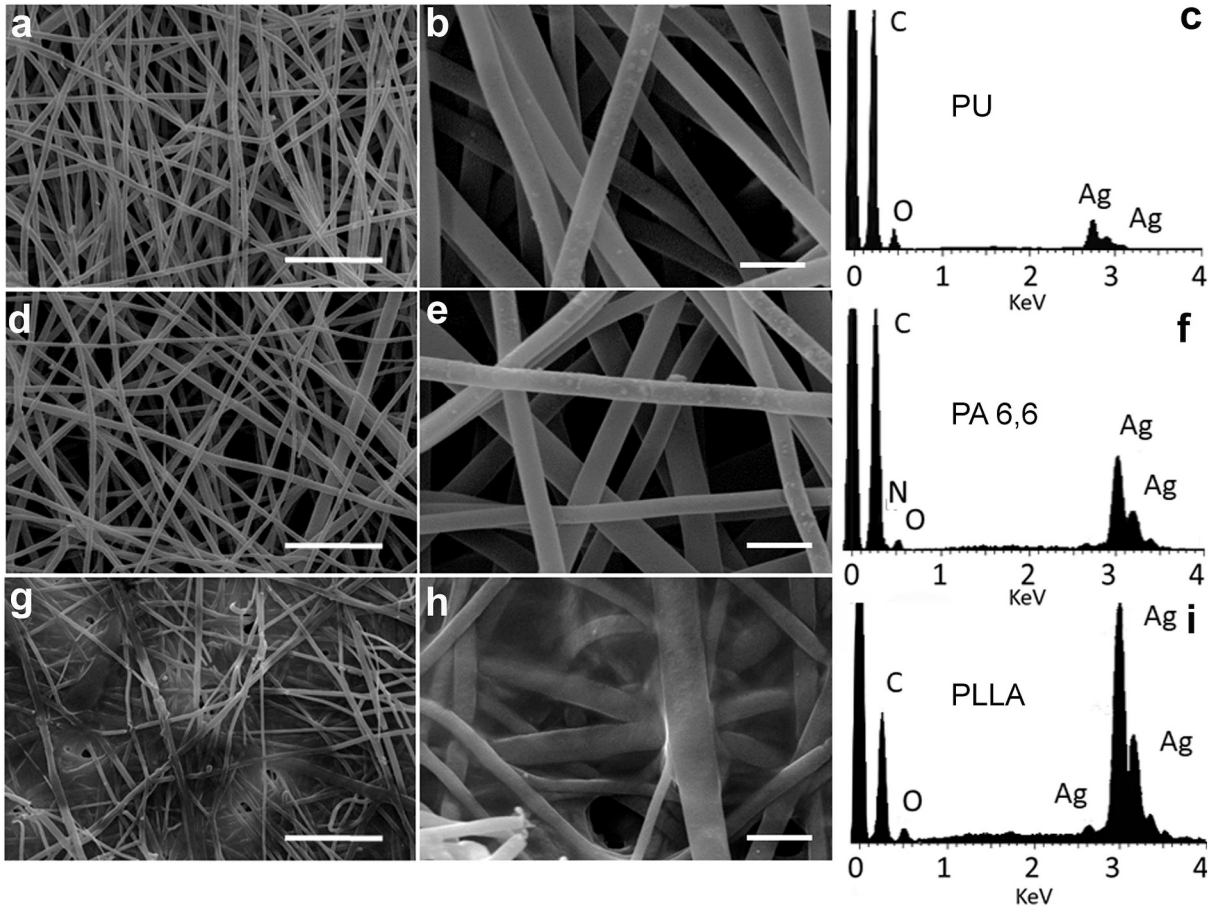

Fig. 2. SEM micrographs of coated electrospun nanofibers: (a, b) Ag-PU, (d, e) Ag-PA 6,6 and (g, h) Ag-PLLA. Scale bars: a, c, e = 10 μm; b, d, f = 3 μm. EDS spectra of Ag-PU (c), Ag-PA 6,6 (f) and Ag-PLLA (i).

within the Ag layer and becomes easier as coating thickness increases due to a decrease of ductility.

AFM investigation allowed to better evaluate the nanostructured topography of the coated fibers compared to uncoated ones (Fig. 3). Despite the impossibility to extract quantitative surface roughness parameters due to the random curvature of the underlying fibers, AFM images pointed out that marked differences exist between the highly smooth surface of the uncoated fibers (Fig. 3d, i, n) and that highly rough of the coated ones. Indeed, silver aggregates composed of grains with size ranging from a few tens to a few hundreds of nanometers were detected on the surface of PU (Fig. 3a–c, e) and PA 6,6 (Fig. 3f–h, j) fibers; smaller silver grains (a few tens of nanometers) were instead randomly dispersed in the PLLA matrix (Fig. 3k–m, o). Taken together, SEM and AFM analyses support the evidence that PU and PA 6,6 are capable to well withstand the deposition treatment without losing their fibrous morphology and porous structure. On the contrary, the capability of PLLA fibers to strongly attract the chemical species generated by the plasma that results in twice the amount of Ag compared to PU and PA 6,6, combined with its fragility (PLLA has half of the stress at break of PU an PA 6,6, Table S1) makes this material more sensitive and less resistant to IJD. However, it is worth noting that by simply reducing the deposition time (from 40 min to 20 min), fibrous morphology of PLLA could be better preserved (Fig. S6).

To evaluate the cohesion of the silver nanocoating, TEM analysis was performed on coated samples after their immersion in a proper solvent capable to solubilize the polymeric component. This treatment was applied to ascertain whether the nanocoating was really cohesive and robust. If this is the case, it is expected that the cylindrical shape of the underlying fibers after the dissolution of the polymeric component is maintained or that the presence of the dense coating prevents polymer dissolution. On the opposite, it is expected that a coating constituted by isolated and not cohesive grains disaggregates after polymer dissolution into the solvent. The results, shown in Fig. 3, highlight the presence of a silver nanocoating structure characterized by compact grains that completely cover the cylindrical surface of the fibers surface. Moreover, the images show that in some cases the coating was thicker on the apical part of the fiber surface, probably the fiber portion closest to the plasma source during the deposition process, while the rest of the surface was covered by a thinner compact coating. Furthermore, from this experiment, it seems that the polymeric components are still present after solvent immersion, probably because the compact coating had prevented the solvent from penetrating into the structure and dissolving the polymers. Another possibility to explain the obtained results is that the IJD treatment had induced some chemical modifications in the polymeric components making them insoluble, as a consequence, for instance, of extended crosslinking reactions. However, the solubility of the uncoated side of the all mats was verified and excluded this hypothesis.

Nevertheless, possible chemical modification of the polymeric counterparts, such as limited crosslinking reactions or bond cleavage, induced by the plasma plume during silver deposition cannot be excluded. ATR-IR analyses carried out on both coated and uncoated sample (Fig. S7) did not highlight any differences before and after silver deposition, since all the spectra present the same peaks with comparable intensity. Therefore, if any chemical changes occurred in the polymers they cannot be detected by IR analysis.

To gain further insights on possible effects of IJD on the different types of investigated polymers, DSC was performed on both uncoated

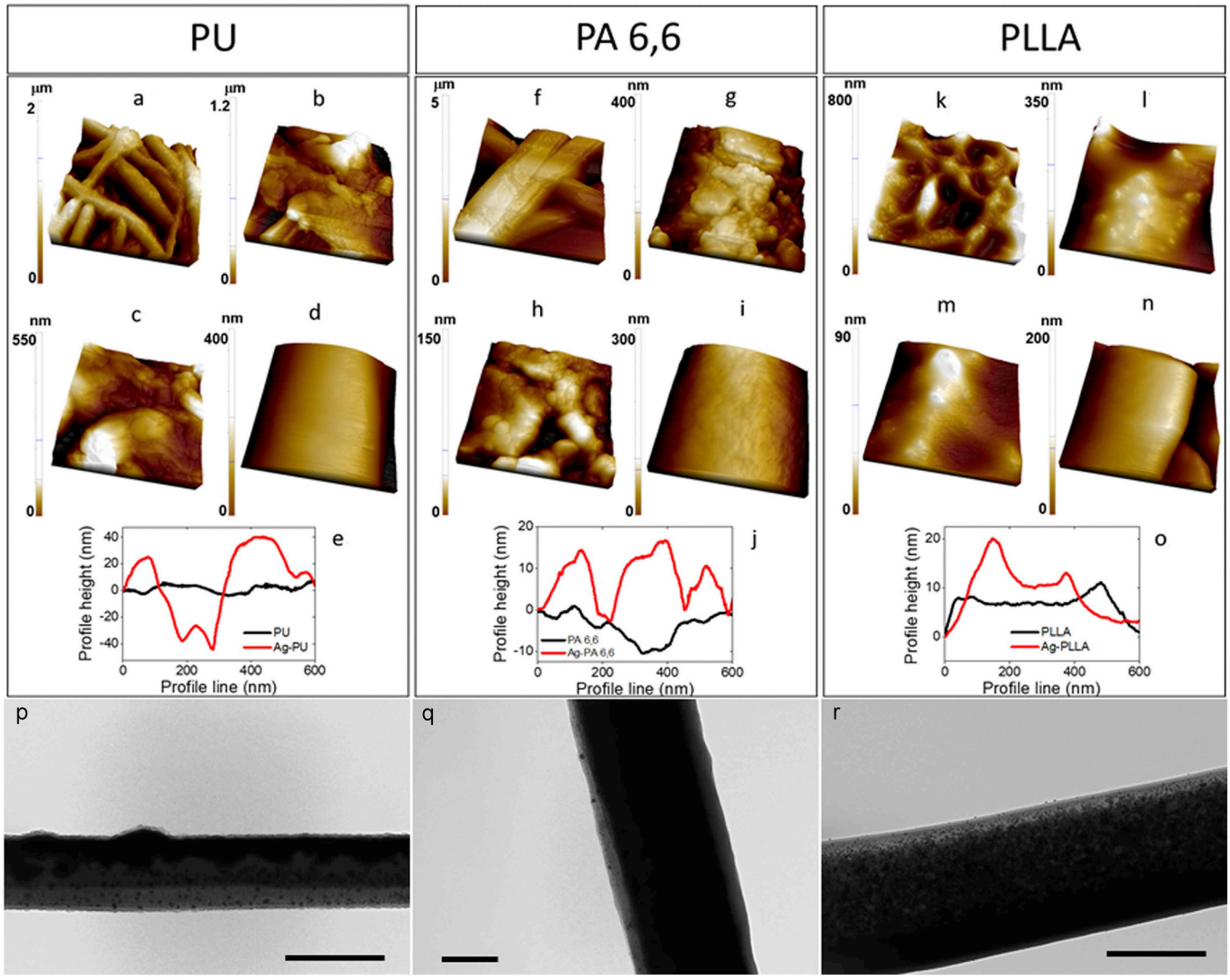

Fig. 3. AFM 3D topography images of coated and uncoated electrospun nanofibers; (a, b, c) Ag-PU; (d) PU; (f, g, h) Ag-PA 6,6; (i) PA 6,6; (k, l, m) Ag-PLLA; (n) PLLA. Image size: 10 × 10 μm^2 (a, f, k), 2 × 2 μm^2 (b, g, l), 0.8 × 0.8 μm^2 (c, d, h, i, m, n). Comparison of line profiles of coated and uncoated fibers for (e) PU samples, (j) PA 6,6 samples and (o) PLLA samples. TEM micrographs of coated electrospun nanofibers previously immersed in a proper solvent to dissolve the polymer: (p) Ag-PU, (q) Ag-PA 6,6 and (r) Ag-PLLA. Scale bars: p, r = 500 nm; q = 200 nm.

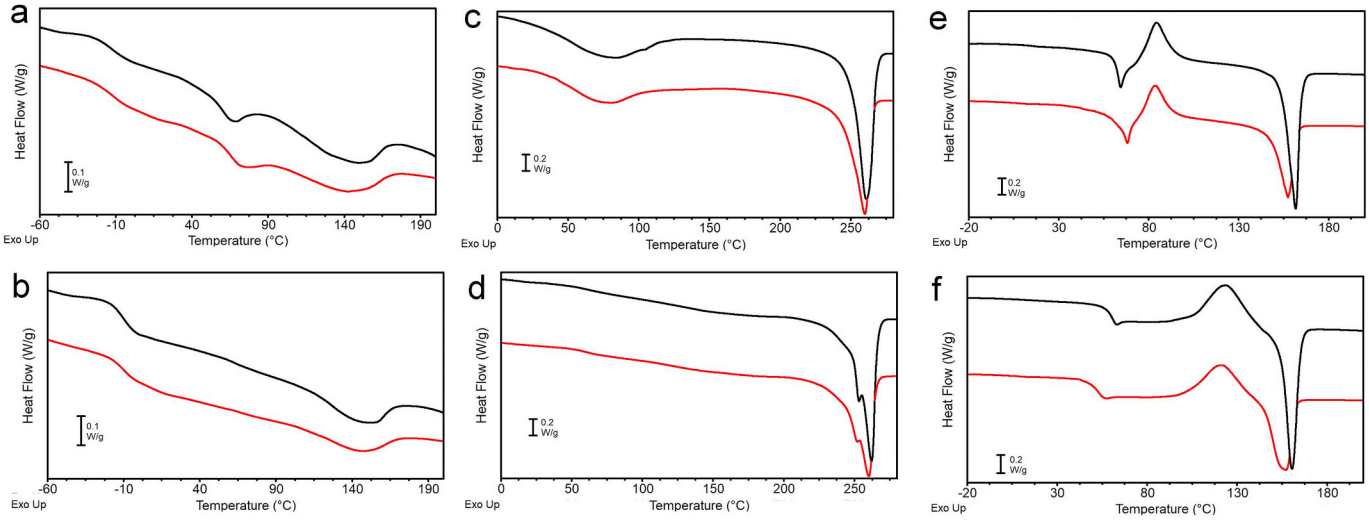

Fig. 4. First (a, c, e) and second heating scan after cooling (b, d, f) of uncoated (black line) and coated (red line) samples: (a, b) PU, (c, d) PA 6,6 and (e, f) PLLA. (For interpretation of the references to colour in this figure legend, the reader is referred to the web version of this article.)

Table 1
Calorimetric data of DSC heating scans of uncoated and coated samples.

Sample	T_g [°C]	ΔC_p [J/g°C]	T_c [°C]	ΔH_c [J/g]	T_m [°C]	ΔH_m [J/g]
1st heating scan						
PU	−13	0.24	–	–	67–143[a]	27
Ag-PU	−13	0.23	–	–	75–143[a]	26
PA 6,6	n.d.[b]	n.d.	–	–	261	75
Ag-PA 6,6	n.d.	n.d.	–	–	260	63
PLLA	n.d.	n.d.	84	36	162	36
Ag-PLLA	n.d.	n.d.	84	25	157	25
2nd heating scan after controlled cooling						
PU	−11	0.30	–	–	145	14
Ag-PU	−11	0.18	–	–	144	10
PA 6,6	58	0.22	–	–	253–262[a]	100
Ag-PA 6,6	59	0.19	–	–	252–260[a]	91
PLLA	59	0.61	124	30	161	37
Ag-PLLA	51	0.55	122	25	157	27

[a] Multiple melting peaks.
[b] n.d. = not detectable.

and coated materials. All samples were subjected to a first heating scan to destroy the thermal history, cooled down below their glass transition temperature (T_g) and reheated. In Fig. 4 both heating scans are reported and the corresponding calorimetric data are listed in Table 1. PU uncoated fibers are semicrystalline, with a T_g below RT and a broad melting region that starts just above RT (T_m onset = 30 °C) characterized by multiple melting peaks with an associated enthalpy ΔH_m = 27 J/g (Fig. 4a). In the second heating scan after cooling (Fig. 4b) the polymer is still semicrystalline but, compared to the first scan, presents a lower value of ΔH_m (14 J/g), indicating a lower amount of crystal phase, but with more homogenous crystals as demonstrated by the sharper melting peak. The thermal transitions of PU were not significantly modified by silver deposition, the most worth noting difference being the onset of melting region in the second scan (T_m onset shifted to 55 °C in Ag-PU) and the consequent increase of the first melting peak T from 67 °C in PU to 75 °C in Ag-PU. This finding might be the consequence of sample annealing occurring during IJD treatment and provides an indication on the maximum temperature reached by the substrate during silver deposition (i.e. 55 °C). PA 6,6 fibers are semicrystalline both in the first and in the second heating scans, with a T_g above RT overlapped, in the first scan, with a broad endotherm peak associated to the evaporation of water typically absorbed by aliphatic polyamides, and a sharp endotherm peak at 261 °C, corresponding to the melting of PA crystal phase (Fig. 4c and d). The coated Ag-PA 6,6 fibers have a similar thermal behavior, the only difference being the lower ΔH_m values measured both in the first and in the second scans compared to the uncoated sample (Table 1), ascribable to the lower weight fraction of polymeric component when silver is present. Differently from PU and PA 6,6, PLLA fibers are completely amorphous after electrospinning, as previously reported [31]. Indeed, the first heating scan of PLLA (Fig. 4e) shows a T_g around 60 °C with an intense enthalpy relaxation peak associated to physical aging, and an exothermal crystallization peak (T_c = 84 °C) followed by a melting endothermic peak (T_m = 162 °C) of the same entity ($\Delta H_c = \Delta H_m$ = 36 J/g). It is worth noting that after IJD treatment PLLA T_g decreased from 59 °C to 51 °C, this is particularly evident in the second heating scan of Ag-PLLA compared to PLLA (Fig. 4f). Concomitantly, melting temperature slightly decreased (from 162 °C to 157 °C). Overall DSC results demonstrates that PU and PA 6,6 are not significantly affected by IJD treatment and preserve their thermal properties. Conversely, DSC of PLLA highlighted a slight decrease of calorimetric parameters occurred after silver deposition. In particular, the decrease of both T_g and T_m in the coated sample can be ascribed to a decrease of polymer molecular weight. In line with this hypothesis, Chu et al. [47] reported for instance that polymers containing oxygen functionalities such as ether, carboxylic acid, and ester groups are highly susceptible to bond scission

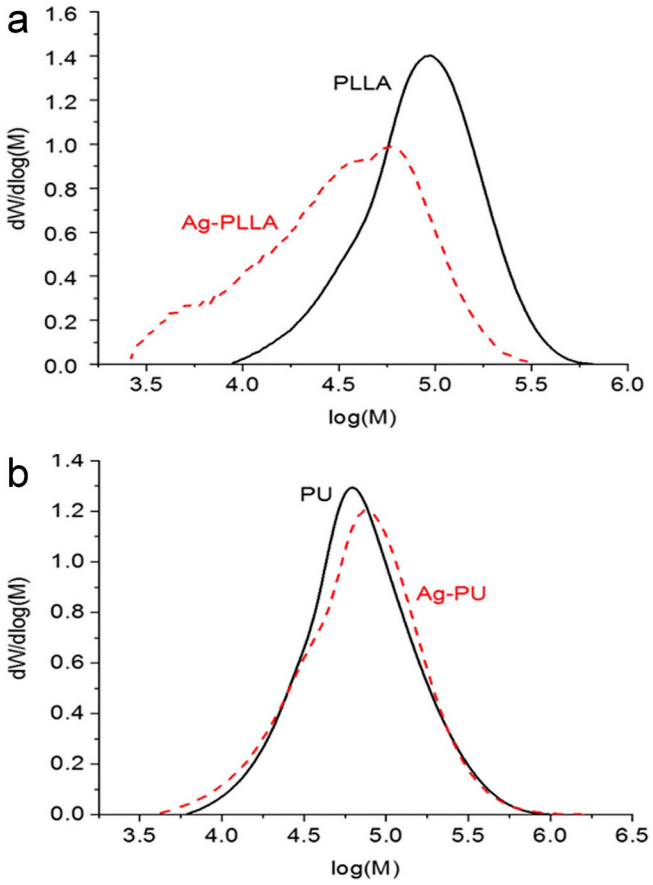

Fig. 5. Molecular weight distributions by GPC of uncoated nonwovens (black solid line) and after IJD treatment (red dotted line): (a) PLLA and (b) PU. (For interpretation of the references to colour in this figure legend, the reader is referred to the web version of this article.)

under ionized plasma. Furthermore, the increase of temperature during IJD treatment, although being modest (i.e. about 55 °C as suggested by Ag-PU annealing), might contribute to accelerate PLLA degradation.

To verify this hypothesis a sample of Ag-PLLA was analyzed by GPC, after carefully peeling out the upper layer of the mat covered by silver. Molecular weight distribution of the coated and uncoated fibers are reported in Fig. 5a. Untreated PLLA displays a monodispersed distribution of molecular weight, with a polydispersity index (PDI) of 1.6 and a weight average molecular weight (M_w) of 104,900 g/mol (Table 2). Differently, Ag-PLLA sample shows a broader molecular weight distribution shifted towards low molecular weight values, with a corresponding PDI of 2.4 and a M_w of 47,300 (Table 2), thus confirming that IJD treatment of 40 min determined a massive decrease of polymer molecular weight, probably due to the cleavage of ester bonds in the polymer main chains. This finding explains the change of polymer thermal behavior and the evident mechanical fragility acquired by the non-woven after the deposition of silver. GPC was also carried out on PU samples (Fig. 5b), while PA 6,6 was not analyzed being not soluble in GPC eluent. GPC analysis revealed that IJD treatment has a minor but evident effect on PU

Table 2
GPC data of PLLA and PU non-wovens, before and after IJD treatment.

Sample	PDI	M_p [g/mol]	M_w [g/mol]
PU	1.8	65,400	93,000
Ag-PU	2.0	81,300	94,900
PLLA	1.6	98,300	104,900
Ag-PLLA	2.4	59,800	47,300

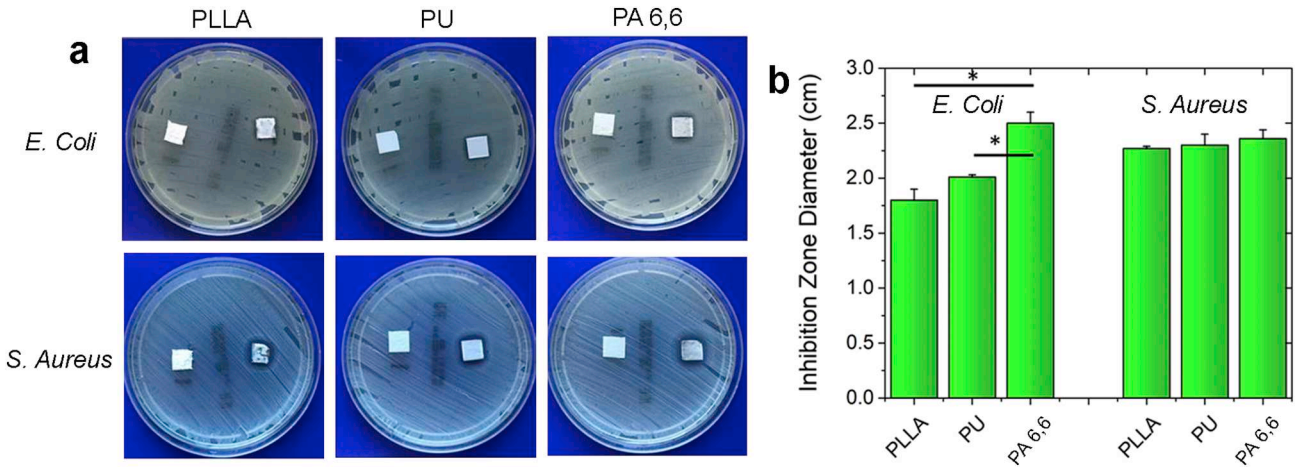

Fig. 6. Results of antibacterial tests. (a) Representative optical images of agar diffusion tests with *E. coli* and *S. aureus* strains performed on the uncoated reference (left patch in every image) and coated (right patch) electrospun mats. (b) Evaluation of the Inhibition Zone Diameter (IZD) after 24 h of incubation in presence of *E. coli* and *S. aureus* (* refers to $p < 0,05$). Please note that while the deposition time is 40 min for Ag-PU and Ag-PA, it is 20 min for Ag-PLLA, as a reduced deposition time was selected to avoid causing damage to the patch.

molecular weight distribution. In particular, the initial monodisperse distribution of PU, characterized by M_w = 93,000 g/mol and PDI = 1.8, changed into a bimodal distribution (PDI = 2.0), with the main peak that shifted towards higher molecular weights (M_p = 81,300 g/mol for Ag-PU and M_p = 65,400 g/mol for PU) and a higher fraction of low molecular weight chains. For this type of polymer, containing ester groups in the soft blocks and aromatic groups in the hard blocks, the occurrence of concomitant crosslinking reactions and bond cleavages during IJD can explain the change of polymer molecular weight distribution, even if these modifications do not compromise the properties of the material.

All the coated electrospun nanofibers exhibited a clear antibacterial efficacy with respect to both gram-negative (*E. coli*) and gram-positive (*S. aureus*), as can be observed by the presence of an inhibition halo around the Ag-coated patches (Fig. 6). In contrast, uncoated mats did not exert any antibacterial effect, as expected. More specifically, overall the efficacy was higher against *S. aureus* with respect to *E. coli*; Ag-PA 6,6 was found to be more effective against *E. coli* compared to Ag-PU and Ag-PLLA whereas all the coated mats exhibited the same antibacterial effect with respect to *S. aureus*. Silver coatings are generally found to exhibit high efficacy against gram negative bacterial strains, while efficacy against gram positive strains, and in particular *S. aureus*, is generally much lower [48,49]. As a consequence, the strong efficacy of silver coated patches against *S. aureus* reported in this study should be remarked. Finally, the presence of the halo also suggested that Ag coatings exerted their antibacterial effect not only by direct contact with bacterial membrane, but also through a diffusion-driven process of silver ions in proximity of the patch. Indeed, it can be conceived that a thin Ag_xO layer is generated on the surface of the Ag films due to spontaneous oxidation in air. Upon immersion of the coated mats in the agar gel, Ag^+ ions, which are commonly believed to be the active antibacterial species [50,51], start to diffuse in the gel, up to few millimeters from the mats, maintaining a local concentration sufficient to inhibit bacterial growth.

4. Conclusions

In this work we proposed a new approach for preparing antibacterial nonwovens by exploiting for the first time the IJD technique to decorate the surface of electrospun fibers with a silver nanostructured coating. All the tested polymeric mats, i.e. PU, PA 6,6 and PLLA, have been successfully covered by a thin and cohesive layer of nanostructured Ag composed of grains with size ranging from a few tens to a few hundreds of nanometers. Further, all the coated mats exhibited significant antibacterial effect against both gram-positive and gram-negative bacterial strains. While PU and PA 6,6 maintained the original fiber morphology after the deposition process, PLLA appeared more sensitive to the coating treatment that, besides altering the fibrous morphology, determined an initial degradation of the polymer chains. However, it was demonstrated that PLLA can be successfully treated with IJD by properly adjusting the time of deposition. Notably, the results of this work demonstrated that the low- temperature IJD process can be applied also to extremely delicate substrates like polymeric submicrometric fibers to endow them with an antibacterial coating. The advantages of this approach over previously reported methods of silver deposition/incorporation are: (i) to accumulate the antibacterial agent (silver) only on the fiber surface, thus being prone to interact with bacteria; (ii) to provide nanostructured coatings, i.e. exhibiting high surface area, thus maximizing the antibacterial efficacy of the material; (iii) to avoid time and solvent consuming chemical treatments; (iv) to be industrially scalable and employable on thermally and chemically susceptible substrates.

CRediT authorship contribution statement

Giorgia Pagnotta: Investigation, Writing - original draft, Visualization, Validation, Formal analysis. **Gabriela Graziani:** Investigation, Methodology, Validation, Writing - review & editing, Project administration. **Nicola Baldini:** Writing - review & editing, Funding acquisition. **Alessandra Maso:** Investigation, Methodology. **Maria Letizia Focarete:** Writing - review & editing, Funding acquisition. **Matteo Berni:** Methodology, Validation, Investigation, Writing - review & editing. **Fabio Biscarini:** Writing - review & editing. **Michele Bianchi:** Conceptualization, Formal analysis, Investigation, Writing - review & editing, Visualization, Supervision, Project administration. **Chiara Gualandi:** Conceptualization, Resources, Writing - original draft, Visualization, Supervision, Project administration.

Declaration of competing interest

None.

Acknowledgments

The Italian Ministry of University and Research (MIUR) is acknowledged. Dr. Gabriela Graziani and Prof. Nicola Baldini kindly

acknowledge 5 per mille funding provided by Istituto Ortopedico Rizzoli for support to the research. Miss. Monica De Carolis (M.D.) is acknowledged for support to silver films deposition, Dr. Elisa Storni and Dr. Elena Donati are acknowledged for collaboration to antibacterial tests.

Appendix A. Supplementary data

Analysis of fiber diameter, mechanical characterization, thermogravimetric analysis, effect of shorter IJD treatment on PLLA microstructure, ATR-IR analysis. Supplementary data to this article can be found online at https://doi.org/10.1016/j.msec.2020.110998.

References

[1] G.A. James, E. Swogger, R. Wolcott, E.D. Pulcini, P. Secor, J. Sestrich, J.W. Costerton, P.S. Stewart, Biofilms in chronic wounds, Wound Repair Regen. 16 (2008) 37–44, https://doi.org/10.1111/j.1524-475X.2007.00321.x.
[2] K. Zheng, M.I. Setyawati, D.T. Leong, J. Xie, Antimicrobial silver nanomaterials, Coord. Chem. Rev. 357 (2018) 1–17, https://doi.org/10.1016/j.ccr.2017.11.019.
[3] P. Aramwit, Introduction to biomaterials for wound healing, Wound Healing Biomaterials 2 (2016) 3–38, https://doi.org/10.1016/B978-1-78242-456-7.00001-5.
[4] B.K. Sun, Z. Siprashvili, P.A. Khavari, Advances in skin grafting and treatment of cutaneous wounds, Science 346 (2014) 941–945, https://doi.org/10.1126/science.1253836.
[5] M. Liu, X.P. Duan, Y.M. Li, D.P. Yang, Y.Z. Long, Electrospun nanofibers for wound healing, Mater. Sci. Eng. C 76 (2017) 1413–1423, https://doi.org/10.1016/j.msec.2017.03.034.
[6] S.P. Miguel, D.R. Figueira, D. Simões, M.P. Ribeiro, P. Coutinho, P. Ferreira, I.J. Correia, Electrospun polymeric nanofibres as wound dressings: a review, Colloids Surfaces B Biointerfaces 169 (2018) 60–71, https://doi.org/10.1016/j.colsurfb.2018.05.011.
[7] R.S. Ambekar, B. Kandasubramanian, Advancements in nanofibers for wound dressing: a review, Eur. Polym. J. 117 (2019) 304–336, https://doi.org/10.1016/j.eurpolymj.2019.05.020.
[8] P. Zahedi, I. Rezaeian, S.O. Ranaei-Siadat, S.H. Jafari, P. Supaphol, A review on wound dressings with an emphasis on electrospun nanofibrous polymeric bandages, Polym. Adv. Technol. 21 (2010) 77–95, https://doi.org/10.1002/pat.1625.
[9] C. Chen, J. Tang, Y. Gu, L. Liu, X. Liu, L. Deng, C. Martins, B. Sarmento, W. Cui, L. Chen, Bioinspired hydrogel electrospun fibers for spinal cord regeneration, Adv. Funct. Mater. 29 (2019) 1–11, https://doi.org/10.1002/adfm.201806899.
[10] H. Chen, Y.S. Lui, Z.W. Tan, J.Y.H. Lee, N.S. Tan, L.P. Tan, Migration and phenotype control of human dermal fibroblasts by electrospun fibrous substrates, Adv. Healthc. Mater. 8 (2019) 1801378, , https://doi.org/10.1002/adhm.201801378.
[11] H. Rodríguez-Tobías, G. Morales, D. Grande, Comprehensive review on electrospinning techniques as versatile approaches toward antimicrobial biopolymeric composite fibers, Mater. Sci. Eng. C 101 (2019) 306–322, https://doi.org/10.1016/j.msec.2019.03.099.
[12] C. Gualandi, A. Celli, A. Zucchelli, M.L. Focarete, Nanohybrid materials by electrospinning, Organic-Inorganic Hybrid Nanomaterials, Springer International Publishing, Cham, 2015, pp. 87–142, , https://doi.org/10.1007/12_2014_281.
[13] Z. Zhang, Y. Wu, Z. Wang, X. Zou, Y. Zhao, L. Sun, Fabrication of silver nanoparticles embedded into polyvinyl alcohol (Ag/PVA) composite nanofibrous films through electrospinning for antibacterial and surface-enhanced Raman scattering (SERS) activities, Mater. Sci. Eng. C 69 (2016) 462–469, https://doi.org/10.1016/j.msec.2016.07.015.
[14] J. An, H. Zhang, J. Zhang, Y. Zhao, X. Yuan, Preparation and antibacterial activity of electrospun chitosan/poly(ethylene oxide) membranes containing silver nanoparticles, Colloid Polym. Sci. 287 (2009) 1425–1434, https://doi.org/10.1007/s00396-009-2108-y.
[15] T.H. Nguyen, K.H. Lee, B.T. Lee, Fabrication of Ag nanoparticles dispersed in PVA nanowire mats by microwave irradiation and electro-spinning, Mater. Sci. Eng. C 30 (2010) 944–950, https://doi.org/10.1016/j.msec.2010.04.012.
[16] Z. Qiao, M. Shen, Y. Xiao, M. Zhu, S. Mignani, J.P. Majoral, X. Shi, Organic/inorganic nanohybrids formed using electrospun polymer nanofibers as nanoreactors, Coord. Chem. Rev. 372 (2018) 31–51, https://doi.org/10.1016/j.ccr.2018.06.001.
[17] X. Zhuang, B. Cheng, W. Kang, X. Xu, Electrospun chitosan/gelatin nanofibers containing silver nanoparticles, Carbohydr. Polym. 82 (2010) 524–527, https://doi.org/10.1016/j.carbpol.2010.04.085.
[18] D.G. Yu, J. Zhou, N.P. Chatterton, Y. Li, J. Huang, X. Wang, Polyacrylonitrile nanofibers coated with silver nanoparticles using a modified coaxial electrospinning process, Int. J. Nanomedicine 7 (2012) 5725–5732, https://doi.org/10.2147/IJN.S37455.
[19] Z. Mao, R. Xie, D. Fu, L. Zhang, H. Xu, Y. Zhong, X. Sui, PAN supported Ag-AgBr@$Bi_{20}TiO_{32}$ electrospun fiber mats with efficient visible light photocatalytic activity and antibacterial capability, Sep. Purif. Technol. 176 (176) (2017) 277–286, https://doi.org/10.1016/j.seppur.2016.12.027.
[20] H.F. Alharbi, M. Luqman, S.T. Khan, Antibiofilm activity of synthesized electrospun core-shell nanofiber composites of PLA and PVA with silver nanoparticles, Mater. Res. Express 5 (2018) 95001, , https://doi.org/10.1088/2053-1591/aad4df.
[21] N.A. Ghavami, A.R. Unnithan, A.R.K. Sasikala, M. Samarikhalaj, R.G. Thomas, Y.Y. Jeong, S. Nasseri, P. Murugesan, D. Wu, C.H. Park, C.S. Kim, Mussel-inspired electrospun nanofibers functionalized with size-controlled silver nanoparticles for wound dressing application, ACS Appl. Mater. Interfaces 7 (2015) 12176–12183, https://doi.org/10.1021/acsami.5b02542.
[22] W. Yang, K. Wu, X. Liu, Y. Jiao, C. Zhou, Construction and characterization of an antibacterial/anticoagulant dual-functional surface based on poly L-lactic acid electrospun fibrous Mats, Mater. Sci. Eng. C 92 (2018) 726–736, https://doi.org/10.1016/j.msec.2018.07.014.
[23] D. Shi, F. Wang, T. Lan, Y. Zhang, Z. Shao, Convenient fabrication of carboxymethyl cellulose electrospun nanofibers functionalized with silver nanoparticles, Cellulose 23 (2016) 1899–1909, https://doi.org/10.1007/s10570-016-0918-x.
[24] D.N. Phan, N. Dorjjugder, M.Q. Khan, Y. Saito, G. Taguchi, H. Lee, Y. Mukai, I.S. Kim, Synthesis and attachment of silver and copper nanoparticles on cellulose nanofibers and comparative antibacterial study, Cellulose 26 (2019) 6629–6640, https://doi.org/10.1007/s10570-019-02542-6.
[25] N. Tra Thanh, M. Ho Hieu, N. Tran Minh Phuong, T. Do Bui Thuan, H. Nguyen Thi Thu, V.P. Thai, T. Do Minh, H. Nguyen Dai, V.T. Vo, H. Nguyen Thi, Optimization and characterization of electrospun polycaprolactone coated with gelatin-silver nanoparticles for wound healing application, Mater. Sci. Eng. C 91 (2018) 318–329, https://doi.org/10.1016/j.msec.2018.05.039.
[26] F.G. Santos, L.C. Bonkovoski, F.P. Garcia, T.S.P. Cellet, M.A. Witt, C.V. Nakamura, A.F. Rubira, E.C. Muniz, Antibacterial performance of a PCL-PDMAEMA blend nanofiber-based scaffold enhanced with immobilized silver nanoparticles, ACS Appl. Mater. Interfaces 9 (2017) 9304–9314, https://doi.org/10.1021/acsami.6b14411.
[27] H.H. Liu, Q. Li, X. Liang, X. Xiong, J. Yu, Z.X. Guo, Antibacterial polycaprolactone electrospun fiber mats prepared by soluble eggshell membrane protein–assisted adsorption of silver nanoparticles, J. Appl. Polym. Sci. 133 (2016) 1–8, https://doi.org/10.1002/app.43850.
[28] J.D. Schiffman, Y. Wang, E.P. Giannelis, M. Elimelech, Biocidal activity of plasma modified electrospun polysulfone mats functionalized with polyethyleneimine-capped silver nanoparticles, Langmuir 27 (2011) 13159–13164, https://doi.org/10.1021/la202605z.
[29] Y. Yang, Z. Zhang, Y. He, Z. Wang, Y. Zhao, L. Sun, Fabrication of Ag@TiO_2 electrospinning nanofibrous felts as SERS substrate for direct and sensitive bacterial detection, Sensors Actuators B Chem. 273 (2018) 600–609, https://doi.org/10.1016/j.snb.2018.05.129.
[30] Y. He, B. Zhou, H. Liang, L. Wang, J. Li, B. Li, Silver nanoparticles on flower-like TiO_2-coated polyacrylonitrile nanofibers: catalytic and antibacterial applications, Colloids Surfaces A Physicochem. Eng. Asp. 529 (2017) 380–386, https://doi.org/10.1016/j.colsurfa.2017.06.025.
[31] C. Gualandi, M. Govoni, L. Foroni, S. Valente, M. Bianchi, E. Giordano, G. Pasquinelli, F. Biscarini, M.L. Focarete, Ethanol disinfection affects physical properties and cell response of electrospun poly(l-lactic acid) scaffolds, Eur. Polym. J. 48 (2012) 2008–2018, https://doi.org/10.1016/j.eurpolymj.2012.09.016.
[32] C. Gualandi, N. Bloise, N. Mauro, P. Ferruti, A. Manfredi, M. Sampaolesi, A. Liguori, R. Laurita, M. Gherardi, V. Colombo, Poly-l-lactic acid nanofiber–polyamidoamine hydrogel composites: preparation, properties, and preliminary evaluation as scaffolds for human pluripotent stem cell culturing, Macromol. Biosci. 16 (2016) 1533–1544, https://doi.org/10.1002/mabi.201600061.
[33] G. Graziani, M. Berni, A. Gambardella, M. De Carolis, M.C. Maltarello, M. Boi, G. Carnevale, M. Bianchi, Fabrication and characterization of biomimetic hydroxyapatite thin films for bone implants by direct ablation of a biogenic source, Mater. Sci. Eng. C 99 (2019) 853–862, https://doi.org/10.1016/j.msec.2019.02.033.
[34] A. Liguori, C. Gualandi, M.L. Focarete, F. Biscarini, M. Bianchi, The pulsed electron deposition technique for biomedical applications: a review, Coatings 10 (2020) 16, https://doi.org/10.3390/coatings10010016.
[35] J. Skočdopole, L. Kalvoda, P. Nozar, M. Netopilík, Preparation of polymeric coatings by ionized jet deposition method, Chem. Pap. 72 (2018) 1735–1739, https://doi.org/10.1007/s11696-018-0426-6.
[36] M. Bianchi, A. Gambardella, G. Graziani, F. Liscio, M. Cristina Maltarello, M. Boi, M. Berni, D. Bellucci, G. Marchiori, F. Valle, Plasma-assisted deposition of bone apatite-like thin films from natural apatite, Mater. Lett. 199 (2017) 32–36, https://doi.org/10.1016/j.matlet.2017.04.005.
[37] M. Bianchi, M. Boi, N. Lopomo, M.C. Maltarello, F. Liscio, S. Milita, A. Visani, A. Russo, M. Marcacci, Nanomechanical characterization of zirconia thin films deposited on Uhmwpe by pulsed plasma deposition, J. Mech. Med. Biol. 15 (2015) 1550070, , https://doi.org/10.1142/S0219519415500700.
[38] M. Bianchi, A. Gambardella, M. Berni, S. Panseri, M. Montesi, N. Lopomo, A. Tampieri, M. Marcacci, A. Russo, Surface morphology, tribological properties and in vitro biocompatibility of nanostructured zirconia thin films, J. Mater. Sci. Mater. Med. 27 (2016) 96, https://doi.org/10.1007/s10856-016-5707-4.
[39] G. Graziani, G. Carnevale, A. Pisciotta, L. Bertoni, M. Boi, A. Gambardella, M. Berni, G. Marchiori, A. Russo, A. De Pol, Pulsed electron deposition of bone-like apatite thin films from a biogenic source: from material characterization to in vitro stem cell differentiation, Orthop. Proc. 100–B (2018) 1, https://doi.org/10.1302/1358-992X.2018.4.001.
[40] D. Bellucci, M. Bianchi, G. Graziani, A. Gambardella, M. Berni, A. Russo, V. Cannillo, Pulsed electron deposition of nanostructured bioactive glass coatings for biomedical applications, Ceram. Int. 43 (2017) 15862–15867, https://doi.org/10.1016/j.ceramint.2017.08.159.
[41] M. Bianchi, L. Degli Esposti, A. Ballardini, F. Liscio, M. Berni, A. Gambardella, S.C.G. Leeuwenburgh, S. Sprio, A. Tampieri, M. Iafisco, Strontium doped calcium phosphate coatings on poly(etheretherketone) (PEEK) by pulsed electron deposition, Surf. Coatings Technol. 319 (2017) 191–199, https://doi.org/10.1016/j.surfcoat.2017.04.012.

[42] A. Gambardella, M. Berni, G. Graziani, A. Kovtun, A. Liscio, A. Russo, A. Visani, M. Bianchi, Nanostructured Ag thin films deposited by pulsed electron ablation, Appl. Surf. Sci. 475 (2019) 917–925, https://doi.org/10.1016/j.apsusc.2019.01.035.

[43] L. Skocdopolova, Device for generating plasma and directing an electron beam towards a target, U.S. Patent Application No. 14/404,365.

[44] C. Gualandi, C.D. Vo, M.L. Focarete, M. Scandola, A. Pollicino, G. Di Silvestro, N. Tirelli, Advantages of surface-initiated ATRP (SI-ATRP) for the functionalization of electrospun materials, Macromol. Rapid Commun. 34 (2013), https://doi.org/10.1002/marc.201200648.

[45] M.K. Khan, J. Luo, R. Khan, J. Fan, Y. Wan, Facile and green fabrication of cation exchange membrane adsorber with unprecedented adsorption capacity for protein purification, J. Chromatogr. A 1521 (2017) 19–26, https://doi.org/10.1016/j.chroma.2017.09.031.

[46] X. Ji, Z. Su, P. Wang, G. Ma, S. Zhang, Polyelectrolyte doped hollow nanofibers for positional assembly of bienzyme system for cascade reaction at O/W interface, ACS Catal. 4 (2014) 4548–4559, https://doi.org/10.1021/cs501383j.

[47] P. Chu, J. Chen, L. Wang, N. Huang, Plasma-surface modification of biomaterials, Mater. Sci. Eng. R Reports 36 (2002) 43–206, https://doi.org/10.1016/S0927-796X(02)00004-9.

[48] W.K. Jung, H.C. Koo, K.W. Kim, S. Shin, S.H. Kim, Y.H. Park, Antibacterial activity and mechanism of action of the silver ion in *Staphylococcus aureus* and *Escherichia coli*, Appl. Environ. Microbiol. 74 (2008) 2171–2178.

[49] M. Guzman, J. Dille, S. Godet, Synthesis and antibacterial activity of silver nanoparticles against Gram-positive and gram-negative bacteria, Nanomedicine Nanotechnology, Biol. Med. 8 (2012) 37–45, https://doi.org/10.1016/j.nano.2011.05.007.

[50] A. Kedziora, M. Speruda, E. Krzyzewska, J. Rybka, A. Łukowiak, G. Bugla-Płoskonska, Similarities and differences between silver ions and silver in nanoforms as antibacterial agents, Int. J. Mol. Sci. 19 (2018) 444, https://doi.org/10.3390/ijms19020444.

[51] J. Dobias, R. Bernier-Latmani, Silver release from silver nanoparticles in natural waters, Environ. Sci. Technol. 47 (2013) 4140–4146, https://doi.org/10.1021/es304023p.